Polymer Chemistry

ARTICLE

A study on the preparation of alkyne functional nanoparticles *via* RAFT emulsion polymerisation.

Pratik Gurnani [a], Alexander B. Cook [a], Robert A. E. Richardson[a], Sébastien Perrier[a,b,c]*

Received 00th January 20xx,
Accepted 00th January 20xx

DOI: 10.1039/x0xx00000x

www.rsc.org/

The multivalent presentation of functional groups on nanoparticle surfaces has long been exploited to attach biologically active moieties. The conventional chemistries typically used (amide, ester, disulfide) however, are non-selective and inefficient. The Huisgen azide alkyne [1,4] cycloaddition (CuAAC) 'click' reaction has paved the way for atom economic, and orthogonal conjugation chemistries, and is now widely used in nanoparticle science. In this work, alkyne functionalised nanoparticles were prepared, without lengthy post-nanoparticle synthesis modification procedures, exploiting RAFT emulsion polymerisations stabilised by functional macro-RAFT agents. Our results indicated that ester derived RAFT agents and addition of pendant charged groups are vital to retain colloidal stability and narrow molecular weight distributions. Finally the nanoparticles and model polymers were functionalised with an azido functional polymer and fluorescent dye, showing the surfaces were easily accessible for rapid and efficient post-polymerisation functionalisation.

Introduction

One of the major advantages exhibited by nanomaterials is their large total surface area (relative to macroscopic materials), which can be modified to present a high density of chemically functional groups. These functional groups can then be modified to introduce new functionality, useful for a variety of applications such as catalysis,[1] anti-fouling[2] and water treatment.[3] In the biomedical field this property has been utilised to great effect, typically by attaching peptides,[4] antibodies[5] and carbohydrates[6] to improve nanoparticle cellular uptake and targeting. Furthermore, it has been shown that nanoparticles conjugated with fluorescent dyes,[7] radiolabels[8] and MRI contrast agents[9, 10] can be used to track nanoparticle *in vivo* distribution, and also act as highly sensitive diagnostic tools. Due to the advances in this area, many researchers have combined these approaches to generate theranostic nanoparticles, combining therapies and diagnostics onto one nanoparticle, which is only achievable due to the high density of surface functionality available for modification.[11, 12] Nonetheless, the typically used chemistries rely on conventional functional groups such as amines,[13] carboxylic acids[14] and thiols,[15] which are not only highly prevalent in biological organisms, but can react non-specifically. Furthermore, commonly used reactions such as carbodiimide amide coupling in aqueous conditions are fraught with side-reactions and low conjugation efficiencies.[16]

Introduced in 2001, the 'click' chemistry concept represents an elegant solution to many of the problems found using conventional coupling techniques. Sharpless and co-workers laid out a set of criteria a 'click' reaction must fulfil, including: being highly yielding; to rapidly create physiologically stable products; have high atom economy; and can be performed in any solvent, especially water.[17] There are now many reactions defined as a 'click', including (but not limited to) thiol-ene/yne coupling,[18] Diels-Alder cycloaddition,[19] oxime coupling[20] and thiol-isocyanate coupling;[21] however perhaps the most iconic, and most widely used, is the copper azide-alkyne [3+2] cycloaddition (CuAAC).[22] This reaction, between an azide and an alkyne, is now heavily used for bioconjugation, as both of the components can be used orthogonally with endogenously found functionalities. This approach therefore represents a facile route to selectively functionalise the surface of nanomaterials, without the drawbacks of the traditional approaches described above. For instance, Bolley *et al*. reported improved functionalisation of superparamagnetic nanoparticles with cyclic RGD integrin binding peptides using copper azide alkyne cycloaddition click techniques over classical carbodiimide amidation reactions.[23] Additionally, the CuAAC reaction has been used to convert otherwise bare gold nanoparticles into glycosylated systems capable of binding to cell surface lectins with azido functional monosaccharides.[6] Due to the orthogonality of these moieties, Brennen *et al*. were able to conjugate acetylene-functionalised *Thermomyces lanuginosus* lipase to azide coated gold nanoparticles *via* the CuAAC reaction, which still retained its enzymatic activity post-conjugation.[24] It should also be noted that other click reactions, such as the ultrafast triazolinedione reaction have been implemented with nano- and micro- particles, and particle functionalisation is not limited to CuAAC.[25]

[a]*Department of Chemistry, University of Warwick, Gibbet Hill Road, Coventry, CV4 7AL, UK*
[b]*Warwick Medical School, University of Warwick, Gibbet Hill Road, Coventry, CV4 7AL, UK*
[c]*Faculty of Pharmacy and Pharmaceutical Sciences, Monash University, 381 Royal Parade, Parkville, VIC 3052, Australia.*
Electronic Supplementary Information (ESI) available: [details of any supplementary information available should be included here]. See DOI: 10.1039/x0xx00000x

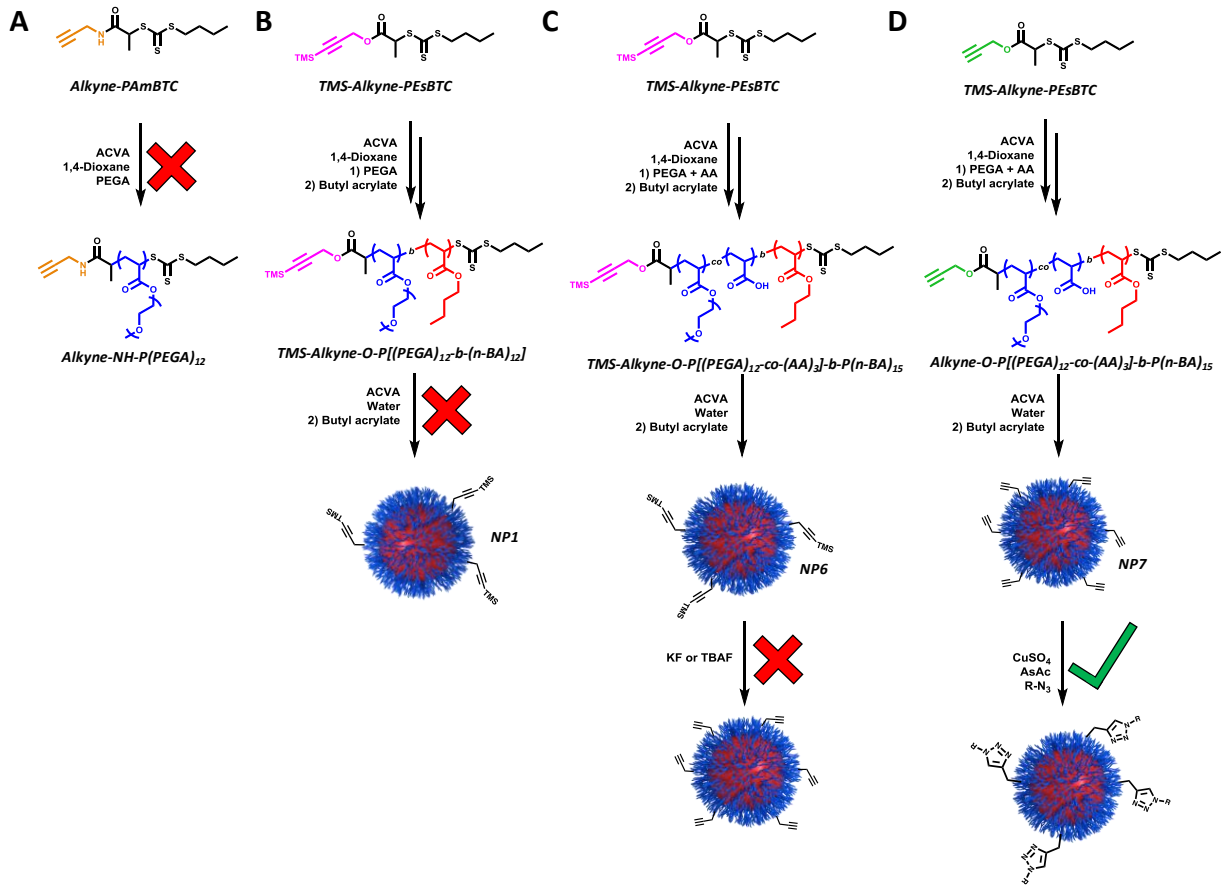

Scheme 1 Unsuccessful synthetic routes (A-C) to alkyne functional nanoparticles using RAFT emulsion polymerisation described within this study. Successful strategy (D) employing ester based RAFT agents and copolymerised acrylic acid in the hydrophilic section of the macro-RAFT agents.

Whilst a large number of substrate conjugations have been demonstrated, it is non-trivial to synthesise nanoparticles bearing the starting azide/alkyne functionalities. One approach to accomplishing this is by utilising RAFT emulsion polymerisation. RAFT emulsion polymerisation combines the advantages of RDRP (narrow molecular weight distributions, controlled molar masses, block copolymers) and emulsion polymerisation (uniform nanoparticles, fast propagation rates and aqueous environments).[26] It operates similarly to traditional emulsion polymerisations, however, the stabiliser is an amphiphilic (preformed or formed *in situ*) macro-RAFT agent forming micelles. These are then chain extended during the polymerisation imparting the hydrophilic stabiliser at the particle corona. A major advantage of RDRP techniques is that there are now many examples of pre-functionalised RDRP initiators (RAFT agents, ATRP initiators etc) with either alkyne or azide groups which after polymerisation would be imparted at the chain ends ready for post-modification.[27] This could therefore be translated to RAFT emulsion polymerisation, through the use of functional macro-RAFT agents, making this an ideal method to generate nanoparticles with high surface functionality. An example of this for nanoparticle functionalisation approach was recently reported by Armes and co-workers, whereby epoxide functionality was introduced either in the pendant chains (copolymerisation of glycidyl methacrylate) or on the end group of the macro-RAFT agent.[28]

It has previously shown that RAFT emulsion polymerisation can be used to introduce carboxylic,[29-35] polysulfonated[36, 37] and biocompatible surfaces.[38] As of yet, this technique has not been used to produce any other surface functionality, including alkynes.

Our aim in this work was therefore to introduce functional alkyne groups on the surface of nanoparticles, by performing RAFT emulsion polymerisations with alkyne functional macro-RAFT agents. These groups would be imparted at the particle surface and therefore be available for reaction/conjugation. Herein we report a synthesis of alkyne functional macro-RAFT agent stabilisers, with three different RAFT agents. Using these stabilisers, RAFT emulsion polymerisations with *n*-butyl acrylate (*n*-BA) were performed to generate alkyne functional nanoparticles. Finally, a CuAAC reaction was performed on both alkyne functional macro-RAFT agents and nanoparticles to assess their post-functionalisation properties.

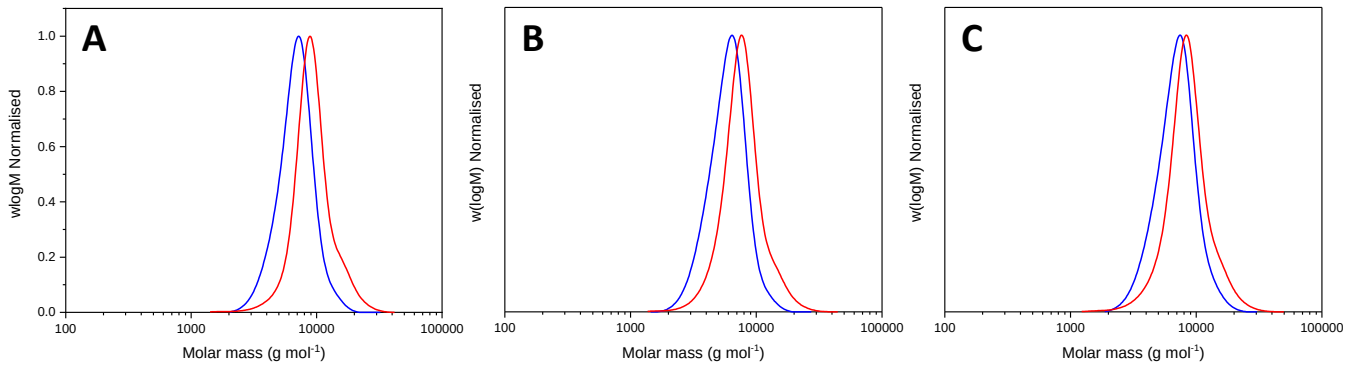

Figure 1 THF-SEC chromatograms of diblock macro-RAFT agents (A) **TMS-Alkyne-O-P[(PEGA)$_{12}$-*b*-(*n*-BA)$_{12}$]** (B) **TMS-Alkyne-O-P[(PEGA)$_{12}$-*co*-(AA)$_3$]-*b*-P(*n*-BA)$_{15}$** (C) **Alkyne-O-P[(PEGA)$_{12}$-*co*-(AA)$_3$]-*b*-P(*n*-BA)$_{15}$,** blue lines indicate the first block (hydrophilic section) and red lines after chain extension with the *n*-BA.

Table 1 **Characterisation data for the polymers (not nanoparticles) synthesised within this study.**

	% conv[a]	$M_{n,th}$ (g mol^{-1})[b]	$M_{n,SEC}$ (g mol^{-1})[c]	$M_{w,SEC}$ (g mol^{-1})[c]	$Đ$[c]
Alkyne-NH-P(PEGA)$_{12}$	89	8800	9800	11550	1.18
TMS-Alkyne-O-P(PEGA)$_{12}$	82	6100	6500	7200	1.11
TMS-Alkyne-O-P[(PEGA)$_{12}$-*b*-(*n*-BA)$_{12}$]	90	7600	8600	9900	1.14
TMS-Alkyne-O-P[(PEGA)$_{12}$-*co*-(AA)$_3$]	84	5900	5500	6200	1.12
TMS-Alkyne-O-P[(PEGA)$_{12}$-*co*-(AA)$_3$]-*b*-P(*n*-BA)$_{15}$	>99	7600	7200	8300	1.15
Alkyne-O-P[(PEGA)$_{12}$-*co*-(AA)$_3$]	87	5350	6500	7400	1.14
Alkyne-O-P[(PEGA)$_{12}$-*co*-(AA)$_3$]-*b*-P(*n*-BA)$_{15}$	81	6900	7800	9100	1.16

[a]Determined using ^{1}H NMR spectroscopy using, [b]Calculated using **Equation 1**, [c]Measured with THF-SEC, calibrated against PMMA standards.

Results and Discussion

Initial optimisation of RAFT agent and macro-RAFT agent composition

As mentioned above, there are no examples of RAFT emulsion polymerisations which impart an reactive functional group, other than carboxylates,[29, 30, 38] at the particle surface. As such, prior to the successful strategy devised (*vide infra*), a number of routes were initially investigated whereby RAFT agent and macro-RAFT agent structure were modified to achieve colloidally stable nanoparticles with narrow molar mass distributions for the comprising polymers. Different alkyne-RAFT agent linkers (amide or ester), protecting group chemistry (presence or absence of trimethylsilyl (TMS)) and the influence of charge on the macro-RAFT agent were studied. The unsuccessful strategies are discussed briefly below and all attempted pathways can be seen in Scheme 1, followed by a detailed section on the optimised route.

Route A – Amide linked alkyne RAFT agent and macro-RAFT agent

Polymerisations targeting a poly(poly(ethylene glycol) methyl ether acrylate) P(PEGA), macro-RAFT agent mediated with RAFT agent **Alkyne-PAmBTC** (characterisation can be found in **Figure S1 and Figure S2**) revealed significant deviations between theoretical and experimental molar masses. This is most obvious during the early stages of the polymerisation (**Table 1**; **Scheme 1a**; **Figure S7d**). Coupled with the low molar mass shoulders in the THF-SEC chromatograms (**Figure S7e)**, we assumed this could be either due to the accessible unprotected alkyne or the 'acrylamide' like reinitiating group on **Alkyne-PAmBTC** not being perfectly suited for acrylate polymerisation**.**

Route B – TMS protected ester linked alkyne

Given that the above pathway failed to produce a suitable diblock stabiliser, a second strategy using a RAFT agent with an ester linkage to a TMS-protected alkyne (**TMS-Alkyne-PEsBTC**; characterisation can be found in **Figure S3** and **Figure S4**) was attempted to circumvent the problems described above. Diblock macro-RAFT agent (**TMS-Alkyne-O-P[(PEGA)$_{12}$-*b*-(*n*-BA)$_{12}$]**) synthesis was indeed successful with **TMS-Alkyne-PEsBTC** (**Figure 1a**, **Table 1**, **Figure S8**) without significant molar mass deviation or low molar mass shoulders in the SEC chromatograms. However, the nanoparticles prepared using previously established RAFT emulsion polymerisation conditions[38], with **TMS-Alkyne-O-P[(PEGA)$_{12}$-*b*-(*n*-BA)$_{12}$]** had a large PDi (0.235) and the dissolved polymers displayed broad molar mass distributions ($Đ$ = 6.51) (**Figure 2a**, **Figure 2f**, **Table 2**). We suspected that the lack of electrostatic stabilisation, was the main cause of this instability, while the hydrophobicity of the trimethylsilyl end-group exacerbated this effect.

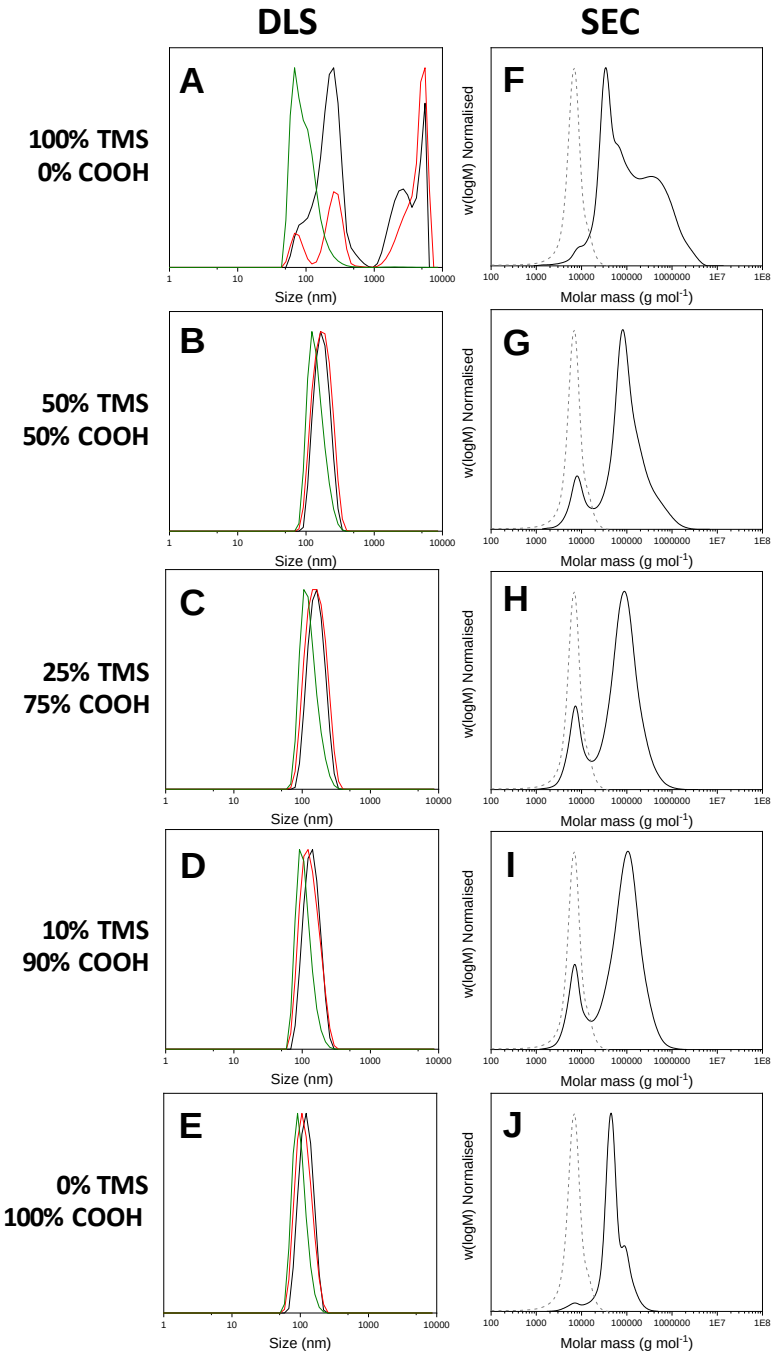

Figure 2 DLS (A-E) and THF-SEC (F-J) traces of *n*-BA RAFT emulsion polymerisations using micelle blends containing various ratios of **COOH-[P(PEGA)$_8$-*b*-P(*n*-BA)$_8$] (COOH)** and **TMS-Alkyne-O-P[(PEGA)$_{12}$-*b*-(*n*-BA)$_{12}$] (TMS)** macro-RAFT agents**.**

To probe this further, RAFT emulsion polymerisations were performed with micelle blends (prepared from thin film rehydration) of the TMS protected macro-RAFT agent (0, 10, 25 and 50 mol%; **TMS-Alkyne-O-P[(PEGA)$_{12}$-*b*-(*n*-BA)$_{12}$])** and a carboxylated derivative (**COOH-P[(PEGA)$_8$-*b*-P(*n*-BA)$_8$];** synthesised in a previous study[38]). Interestingly, a clear decreasing trend in particle diameter was observed with an increasing amount of carboxylated **COOH-P[(PEGA)$_8$-*b*-P(*n*-BA)$_8$]** macro-RAFT agent (143.6, 129.0, 108.6, 99.1 nm for 50, 25, 10 and 0% respectively; **Figure 2b-j**). These latexes displayed far narrower *PDi* values (< 0.1), suggesting improved colloidal stability (**Figure 2b-e**). As expected, zeta-potentials of the nanoparticle became increasingly negative, with increasing amounts of **COOH-P[(PEGA)$_8$-*b*-P(*n*-BA)$_8$]** present in the RAFT emulsion polymerisations (**Table 2; NP2-5**). Nonetheless, as with the 100% TMS macro-RAFT agent polymerisations, broad molar mass distributions were observed for reactions conducted with 50, 25 and 10 % TMS macro-RAFT agent (**Figure 2g-i**; $Đ$ ~ 4.5). However, the polymerisation with no TMS macro-

Table 2 Characterisation data for nanoparticles (and their dissolved unimers) synthesised in this study. Mixtures refer to molar concentration of **TMS-Alkyne-O-P[(PEGA)$_{12}$-*b*-(*n*-BA)$_{12}$]-*b*-P(*n*-BA)$_{200}$** and **COOH-P[(PEGA)$_8$-*b*-(*n*-BA)$_8$]-*b*-P(*n*-BA)$_{200}$** of micelle blends.

		Mixtures (%)	pH	D_h[a] (nm)	*PDi*[b]	*ZP*[c] (mV)	$M_{n,th}$ (g mol^{-1})[d]	$M_{n,SEC}$ (g mol^{-1})[e]	$M_{w,SEC}$ (g mol^{-1})[e]	*Đ*[e]
NP1	**TMS-Alkyne-O-P[(PEGA)$_{12}$-*b*-(*n*-BA)$_{12}$]-*b*-P(*n*-BA)$_{200}$** **COOH-P[(PEGA)$_8$-*b*-(*n*-BA)$_8$]-*b*-P(*n*-BA)$_{200}$**	**100%** **0%**	7.2	100	0.235	-1.5	32,500	48100	313100	6.51
NP2	**TMS-Alkyne-O-P[(PEGA)$_{12}$-*b*-(*n*-BA)$_{12}$]-*b*-P(*n*-BA)$_{200}$** **COOH-P[(PEGA)$_8$-*b*-(*n*-BA)$_8$]-*b*-P(*n*-BA)$_{200}$**	**50%** **50%**	4.9	144	0.083	-11.7	32,500	32800	147300	4.49
NP3	**TMS-Alkyne-O-P[(PEGA)$_{12}$-*b*-(*n*-BA)$_{12}$]-*b*-P(*n*-BA)$_{200}$** **COOH-P[(PEGA)$_8$-*b*-(*n*-BA)$_8$]-*b*-P(*n*-BA)$_{200}$**	**25%** **75%**	4.5	129	0.091	-22.6	32,500	24400	99100	4.06
NP4	**TMS-Alkyne-O-P[(PEGA)$_{12}$-*b*-(*n*-BA)$_{12}$]-*b*-P(*n*-BA)$_{200}$** **COOH-P[(PEGA)$_8$-*b*-(*n*-BA)$_8$]-*b*-P(*n*-BA)$_{200}$**	**90%** **10%**	4.4	109	0.075	-29.4	32,500	24900	106600	4.28
NP5	**TMS-Alkyne-O-P[(PEGA)$_{12}$-*b*-(*n*-BA)$_{12}$]-*b*-P(*n*-BA)$_{200}$** **COOH-P[(PEGA)$_8$-*b*-(*n*-BA)$_8$]-*b*-P(*n*-BA)$_{200}$**	**0%** **100%**	4.2	99	0.059	-40.2	32,500	36300	58800	1.62
NP6	**TMS-Alkyne-O-P{[(PEGA)$_{12}$-*co*-(AA)$_3$-*b*-(*n*-BA)$_{15}$]-*b*-P(*n*-BA)$_{200}$}**	-	3.9	101	0.055	-49.5	33,200	33,000	64,000	1.92
NP7	**Alkyne-O-P{[(PEGA)$_{12}$-*co*-(AA)$_3$-*b*-(*n*-BA)$_{15}$]-*b*-P(*n*-BA)$_{200}$}**	-	4.5	54	0.065	-52.1	33,100	37,000	78,400	2.12

[a]Determined using dynamic light scattering, [b]Calculated using **Equation 2**, [c]Measured with a zetasizer, calibrated against PMMA standards. [d]Calculated using **Equation 1**. [e]Measured with THF-SEC, calibrated against PMMA standards.

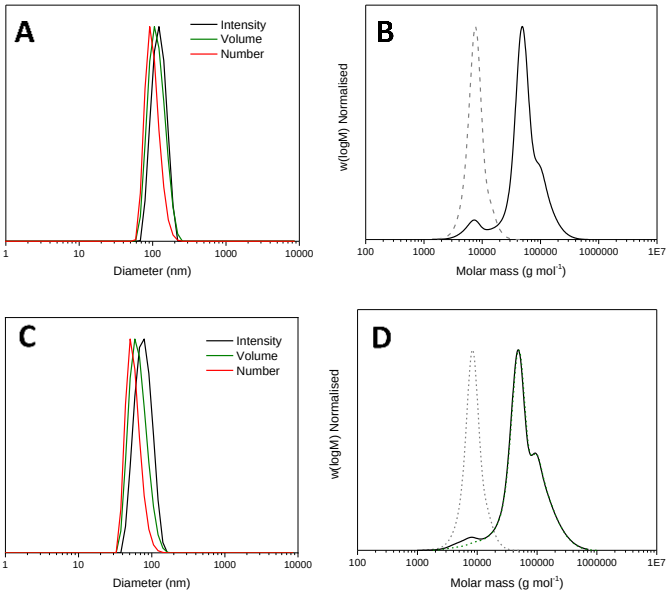

Figure 3 DLS traces (black = intensity, green = volume, red = number) of nanoparticles of **NP6** (A) and **NP7** (C). THF-SEC (grey dashed line = macro-RAFT agent, black line = before dialysis, green dashed line, after dialysis) of polymeric unimers (after dissolving in THF) synthesised from RAFT emulsion polymerisations using **TMS-Alkyne-*O*-{P[(PEGA)$_{13}$-*co*-(AA)$_3$]-*b*-P(*n*-BA)$_{15}$}** (B) **Alkyne-O-{P[(PEGA)$_{12}$-*co*-(AA)$_3$]-*b*-P(*n*-BA)$_{15}$}** (D).

RAFT agent (i.e 100% carboxylated macro-RAFT agent **COOH-P[(PEGA)$_8$-*b*-P(*n*-BA)$_8$]**, yielded a narrower molar mass distribution (*Đ* = 1.62; **Figure 2i**). These observations supported our previous hypothesis, suggesting the TMS protecting group was interfering with the colloidal stability and RAFT emulsion polymerisation. Similar observations were recently reported by Lansalot and co-workers using hydrophobic naphthalene functionalised macro-RAFT agents.[39] Although, stable latexes with narrow *PDi* values were obtained with 10, 25 and 50% TMS macro-RAFT agent, the poor molar mass distributions observed could indicate poor consumption of the macro-RAFT agent, and subsequently low level of alkyne functionality at the nanoparticle surface.

Route C – Incorporation of carboxylate groups for electrostatic stabilisation

The clear improvement in colloidal stability and molar mass distribution after introducing carboxylate groups into the RAFT emulsion polymerisations led us to the conclusion that electrostatic stabilisation was imperative for successful polymerisation. As such, RAFT emulsion polymerisations using an analogous TMS protected macro-RAFT agent (**Figure 1b**) with pendant carboxylic acids (acrylic acid), **TMS-Alkyne-O-P[(PEGA)$_{12}$-*co*-(AA)$_3$]**, were performed. DLS analysis showed that the formation of 101 nm nanoparticles with a much narrower particle size distribution (*PDi* = 0.055; **Figure 3a**). The resulting polymer (**Figure 3b**) had a narrower (but still broad due to the low and high molar mass shoulders) dispersity (*Đ*=1.92) as compared to those where no acrylic acid was present in the macro-RAFT agent (**Figure 2F**; **Table 2**).

Unfortunately, full removal of the TMS protecting groups on the nanoparticles using potassium was unsuccessful in an aqueous environment when analysed with ^{1}H NMR spectroscopy (**Figure S11a**). Furthermore, deprotection attempts on the TMS protected macro-RAFT agent as a model with both KF and tetra-butyl ammonium fluoride (TBAF) in organic solvent were also only partially successful, and as such the protecting group approach was abandoned (**Figure S11b**).

Improving colloidal stability and molar mass distribution

Route D – Unprotected ester linked alkyne macro-RAFT agents with electrostatic stabilisation

The results from the three synthesis routes presented above clearly show that an ester based RAFT agent is required to

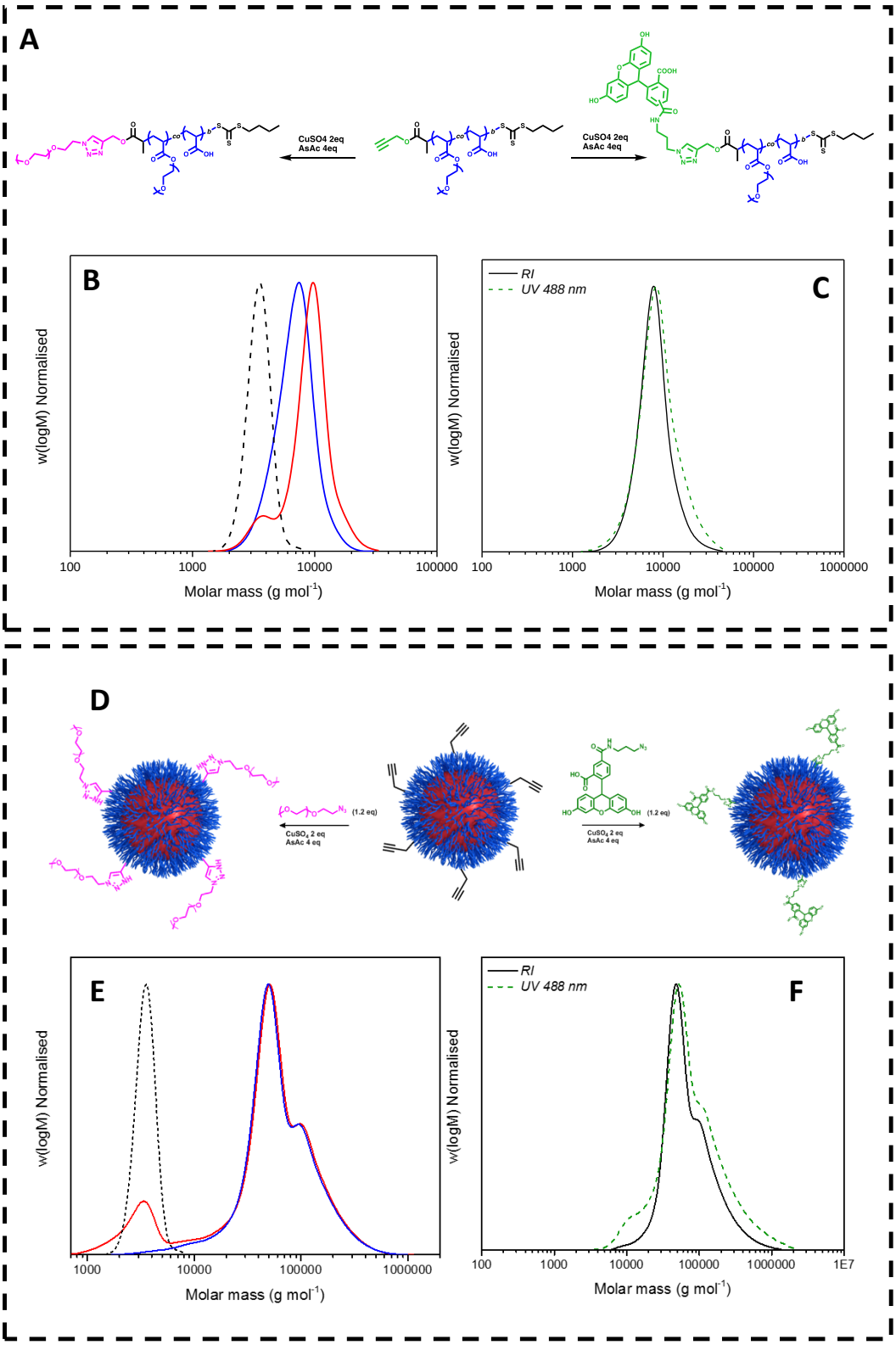

Figure 4 **Synthetic schemes for CuAAC reaction between** PEG-2k-N_3 **or** Fluorescein-N_3 **and (A)** Alkyne-O-P[$(PEGA)_{12}$-co-$(AA)_3$] **and (D) Alkyne functional nanoparticles. THF-SEC chromatograms of before (blue line) and after (red line) CuAAC reactions with** PEG-2k-N_3 **(black dashed line) on (B)** Alkyne-O-P[$(PEGA)_{12}$-co-$(AA)_3$] **and the alkyne functional nanoparticles (E). THF-SEC chromatograms monitored with RI (black line) and** $UV_{488\ nm}$ **(green dashed line) after CuAAC reactions between** Fluorescein-N_3 **and (C)** Alkyne-O-P[$(PEGA)_{12}$-co-$(AA)_3$] **or (F) the alkyne functional nanoparticles.**

produce controlled molecular weight macro-RAFT agents. Furthermore, the addition of negative charge in the pendant chain of the nanoparticle shell is necessary to maintain colloidal stability. We envisaged that the inefficient polymerisation with **Alkyne-PAmbTC** could solely be due to the amide reinitiating group, and not the presence of a terminal alkyne, which has been implemented in many other studies.[40-42] With the unsuccessful deprotection of the TMS-alkyne coated nanoparticles with KF, a non-protected analogue of **TMS-Alkyne-PEsBTC** was synthesised, retaining the ester R group for more efficient initiation.

Alkyne-PEsBTC was synthesised according to the conditions described in a literature procedure,[43] and an analogous non-protected alkyne functional macro-RAFT agent to **TMS-Alkyne-*O*-{P[(PEGA)$_{13}$-*co*-(AA)$_3$]-*b*-P(*n*-BA)$_{15}$}** was prepared *via* a two-step polymerisation (**Scheme 1d**). Both blocks had narrow molar mass distributions ($Đ$ < 1.2), with similar $M_{,th}$ and $M_{n,SEC}$ (**Table 1**). Additionally a significant shift towards higher molar mass was evident, indicating successful chain extension (**Figure 1c**). Although the terminal alkyne was not protected during the polymerisation, no low molecular weight shoulder or broadening was observed, suggesting the alkyne did not get consumed in the reaction. Furthermore comparing the ^{1}H NMR spectrum of **Alkyne-PEsBTC** and **Alkyne-O-{P[(PEGA)$_{12}$-*co*-(AA)$_3$]-*b*-(*n*-BA)$_{15}$}** the singlet, at 4.6 ppm attributed to the CH_2 adjacent to the acetylene group, was retained, confirming this theory (**Figure S10**). It is likely therefore that the poor molecular weight control when using **Alkyne-PAmBTC** was mainly attributed to the amide reinitiating group as previously described, and not the unprotected alkyne.

RAFT emulsion polymerisation with non-protected alkyne macro-RAFT agent

Using the conditions described above, a RAFT emulsion polymerisation was performed using the non-protected alkyne macro-RAFT agent, **Alkyne-O-{P[(PEGA)$_{12}$-*co*-(AA)$_3$]-*b*-P(*n*-BA)$_{15}$}**, as before targeting a DP of 200, to produce non-protected alkyne functional nanoparticles (**Scheme 1d; NP7**). Interestingly, the particles produced with this non-protected macro-RAFT agent had a far smaller diameter (54 nm; **Figure 3c**) than those extended from the TMS protected derivative (101 nm; **Figure 3a**). This is likely due to the increased surface hydrophilicity and electrostatic stability without the TMS protecting group (i.e better surfactant activity) and with the acrylic acid moieties respectively. As before, SEC analysis revealed a high chain extension efficiency and a relatively narrow dispersity compared to those obtained with the macro-RAFT agent without acrylic acid, and with the hydrophobic TMS group. Furthermore similar $M_{n,th}$ and the obtained $M_{n,SEC}$ were observed (33100 and 37000 g mol^{-1} respectively) indicating good molecular weight control (**Figure 3d**).

Prior to any CuAAC reactions directly on the nanoparticles, the latex was dialysed to remove any unconsumed macro-RAFT agent, resulting in a reduction of the lower molar mass region in the size exclusion chromatogram (**Figure 3d**). This is of particular importance, as the residual macro-RAFT agent also had alkyne functionality and may compete against the acetylene groups at the nanoparticle surface during a CuAAC reaction.

CuAAC reactions

On model polymers

Although the above ^{1}H NMR spectra (**Figure S10**) indicates the presence of an alkyne, the large steric bulk from the P(PEGA chains) may make this functionality inaccessible for further reactions. We envisaged that an azido functional fluorescent dye could be used as a model molecule in a CuAAC conjugation reaction and the reaction could be monitored via UV detection SEC to observe the conjugated fluorescein. Using previously described conditions, a CuAAC reaction was performed on **Alkyne-O-P[(PEGA)$_{12}$-co-(AA)$_3$]** with **Fluorescein-N$_3$** using copper sulfate as the Cu(II) source, and ascorbic acid as a reducing agent to generate Cu(I) in situ (**Figure 4a**).[44] After the reaction, a clear overlap between the RI and UV$_{488}$ nm (488 nm is the absorbance maxima of fluorescein; **Figure 4c**) traces could be observed, suggesting Fluorescein-N$_3$ had been conjugated. As some potential azide substrates may be larger than small molecules, the CuAAC reaction was further investigated using a 2 kDa azido function PEG (**PEG-2k-N$_3$**) and the same conditions as above (**Figure 4d**). The reaction was monitored using SEC, and after 2 h stirring at room temperature a clear shift towards higher molar mass (6500 g mol-1 for **Alkyne-O-P[(PEGA)$_{12}$-co-(AA)$_3$]** to 8000 g mol-1 for **PEG-2k-P[(PEGA)$_{12}$-co-(AA)$_3$])** was observed suggesting successful conjugation (**Figure 4b**). A residual amount of **PEG-2k-N$_3$** was observed as a low molar mass shoulder, and is likely the extra 0.2 eq present at the end of the reaction or incomplete conversion. Overall these results suggest that after producing the macro-RAFT agent with a non-protected alkyne end-group, it is still available for post polymerisation modification.

On alkyne functional nanoparticles

Similar CuAAC reactions with both **PEG-2k-N$_3$** and **Fluorescein-N$_3$** were performed with the above alkyne functional nanoparticles, assuming that 100% of the macro-RAFT agent, and therefore alkyne moieties which were available at the particle surface. After addition of the azido functional PEG, no shift in the SEC was observed, while some of the **PEG-2k-N$_3$** could still be seen at lower molar mass, likely due to incomplete conversion (**Figure 4e**). As in the CuAAC reactions with the model polymer, after addition of **Fluorescein-N$_3$** to the nanoparticles in the presence of $CuSO_4$ and ascorbic acid, a clear overlap could be observed between the RI and UV$_{488}$ nm channel (**Figure 4f**). These results indicate **Fluorescein-N$_3$** had been successfully clicked onto the nanoparticles. However, any cycloaddition which did occur may not be detectable *via* SEC due to the small increase in molar mass in comparison to the original trace before reaction.

Conclusions

In conclusion, through a systematic polymerisation study using three different alkyne functional RAFT agents (amide coupled, ester coupled and TMS protected ester coupled), we have investigated the requirements for generating alkyne functional nanoparticles *via* RAFT emulsion polymerisation. Our results indicate that the presence of an amide bond at the reinitiating group severely reduces molecular weight control. Furthermore, protection of terminal alkynes throughout the synthesis is not required to generate low dispersity macro-RAFT agent stabilisers. However, protection/removal of the carboxylate end-group dramatically impacts the colloidal stability of the nanoparticles. This was overcome by reintroducing this functionality into the side chain by copolymerisation of acrylic acid into the hydrophilic block of the stabilising macro-RAFT agent. Finally, we showed that the resultant alkyne functional nanoparticles could be post-modified with either an azido-functional linear PEG or fluorescein azide. This methodology is an effective process to introduce functionality at the nanoparticle surface.

Conflicts of interest

There are no conflicts to declare

Acknowledgements

The authors thank CRUK/EPSRC (C53561/A19933; P.G., S.P.) and the Royal Society Wolfson Merit Award (WM130055; S.P.) for financial support.

References

1 1. L. Pasquato, P. Pengo and P. Scrimin, *Supramol. Chem.*, 2005, 17, 163-171.
2 2. K. C. Anyaogu, A. V. Fedorov and D. C. Neckers, *Langmuir*, 2008, 24, 4340-4346.
3 3. H. Qian, L. A. Pretzer, J. C. Velazquez, Z. Zhao and M. S. Wong, *J. Chem. Technol. Biotechnol.*, 2013, 88, 735-741.
4 4. J. Zong, S. L. Cobb and N. R. Cameron, *Biomaterials Science*, 2017, 5, 872-886.
5 5. L. Feng, L. Liu, F. Lv, G. C. Bazan and S. Wang, *Adv. Mater.*, 2014, 26, 3926-3930.
6 6. V. Poonthiyil, T. K. Lindhorst, V. B. Golovko and A. J. Fairbanks, *Beilstein Journal of Organic Chemistry*, 2018, 14, 11-24.
7 7. R. Serrano García, S. Stafford and Y. Gun'ko, *Applied Sciences*, 2018, 8, 172.
8 8. K. Stockhofe, J. M. Postema, H. Schieferstein and T. L. Ross, *Pharmaceuticals*, 2014, 7, 392-418.
9 9. L. c. Moriggi, C. Cannizzo, E. Dumas, C. d. R. Mayer, A. Ulianov and L. Helm, *J. Am. Chem. Soc.*, 2009, 131, 10828-10829.
10 10. L. Esser, N. P. Truong, B. Karagoz, B. A. Moffat, C. Boyer, J. F. Quinn, M. R. Whittaker and T. P. Davis, *Polymer Chemistry*, 2016, 7, 7325-7337.
11 11. S. M. Janib, A. S. Moses and A. J. MacKay, *Adv. Drug Del. Rev.*, 2010, 62, 1052-1063.
12 12. N. Ahmed, H. Fessi and A. Elaissari, *Drug Discovery Today*, 2012, 17, 928-934.
13 13. H. Wang, J. Zhuang and S. Thayumanavan, *ACS Macro Letters*, 2013, 2, 948-951.
14 14. S. Chen and K. Kimura, *Langmuir*, 1999, 15, 1075-1082.
15 15. E. D. H. Mansfield, K. Sillence, P. Hole, A. C. Williams and V. V. Khutoryanskiy, *Nanoscale*, 2015, 7, 13671-13679.
16 16. N. Nakajima and Y. Ikada, *Bioconjugate Chem.*, 1995, 6, 123-130.
17 17. H. C. Kolb, M. G. Finn and B. K. Sharpless, *Angew. Chem. Int. Ed.*, 2001, 40, 2004-2021.
18 18. A. B. Lowe, C. E. Hoyle and C. N. Bowman, *J. Mater. Chem.*, 2010, 20, 4745-4750.
19 19. M. Tasdelen, *Polymer Chemistry*, 2011, 2, 2133-2145.
20 20. S. Ulrich, D. Boturyn, A. Marra, O. Renaudet and P. Dumy, *Chemistry - A European Journal*, 2014, 20, 34-41.
21 21. H. Li, B. Yu, H. Matsushima, C. E. Hoyle and A. B. Lowe, *Macromolecules*, 2009, 42, 6537-6542.
22 22. R. Huisgen, *Angew. Chem. Int. Ed.*, 1963, 2, 565-598.
23 23. J. Bolley, E. Guenin, N. Lievre, M. Lecouvey, M. Soussan, Y. Lalatonne and L. Motte, *Langmuir*, 2013, 29, 14639-14647.
24 24. J. L. Brennan, N. S. Hatzakis, R. T. Tshikhudo, V. Razumas, S. Patkar, J. Vind, A. Svendsen, R. J. M. Nolte, A. E. Rowan and M. Brust, *Bioconjugate Chem.*, 2006, 17, 1373-1375.
25 25. R. Absil, S. Çakir, S. Gabriele, P. Dubois, C. Barner-Kowollik, F. Du Prez and L. Mespouille, *Polymer Chemistry*, 2016, 7, 6752-6760.
26 26. P. B. Zetterlund, S. C. Thickett, S. Perrier, E. Bourgeat-Lami and M. Lansalot, *Chem. Rev.*, 2015, 115, 9745-9800.
27 27. U. Mansfeld, C. Pietsch, R. Hoogenboom, R. C. Becer and U. S. Schubert, *Polymer Chemistry*, 2010, 1, 1560-1598.
28 28. C. György, J. R. Lovett, N. J. W. Penfold and S. P. Armes, *Macromol. Rapid Commun.*, 0, 1800289.
29 29. C. Poon, O. Tang, X.-M. Chen, B. T. T. Pham, G. Gody, C. A. Pollock, B. S. Hawkett and S. Perrier, *Biomacromolecules*, 2016, 17, 965-973.
30 30. C. Poon, O. Tang, X. M. Chen, B. Kim, M. Hartlieb, C. A. Pollock, B. S. Hawkett and S. Perrier, *Macromol. Biosci.*, 2017, 17, 1600366.
31 31. I. Chaduc, A. Crepet, O. Boyron, B. Charleux, F. D'Agosto and M. Lansalot, *Macromolecules*, 2013, 46, 6013-6023.
32 32. I. Chaduc, M. Girod, R. Antoine, B. Charleux, F. D'Agosto and M. Lansalot, *Macromolecules*, 2012, 45, 5881-5893.
33 33. M. Chenal, L. Bouteiller and J. Rieger, *Polym. Chem.*, 2013, 4, 752-762.
34 34. J. Lesage de la Haye, I. Martin-Fabiani, M. Schulz, J. L. Keddie, F. D'Agosto and M. Lansalot, *Macromolecules*, 2017, 50, 9315-9328.
35 35. A. A. Cockram, R. D. Bradley, S. A. Lynch, P. C. D. Fleming, N. S. J. Williams, M. W. Murray, S. N. Emmett and S. P. Armes, *Reaction Chemistry & Engineering*, 2018, 3, 645-657.
36 36. P. Gurnani, C. P. Bray, R. A. E. Richardson, R. Peltier and S. Perrier, *Macromol. Rapid Commun.*, 2018, DOI: 10.1002/marc.201800314.
37 37. E. Velasquez, J. Rieger, F. Stoffelbach, F. D'Agosto, M. Lansalot, P.-E. Dufils and J. Vinas, *Polymer*, 2016, 106, 275-284.
38 38. P. Gurnani, C. Sanchez-Cano, K. Abraham, H. Xandri-Monje, A. B. Cook, M. Hartlieb, F. Lévi, R. Dallmann and S. Perrier, *Macromol. Biosci.*, 2018, DOI: 10.1002/mabi.201800213.
39 39. B. Ebeling, K. Belal, F. Stoffelbach, P. Woisel, M. Lansalot and F. D'Agosto, *Macromol. Rapid Commun.*, 0, 1800455.
40 40. J. R. Góis, A. V. Popov, T. Guliashvili, A. C. Serra and J. F. J. Coelho, *RSC Advances*, 2015, 5, 91225-91234.
41 41. M. Le Bohec, S. Piogé, S. Pascual and L. Fontaine, *J. Polym. Sci., Part A: Polym. Chem.*, 2017, 55, 3597-3606.

42 42. K. Luo, J. Yang, P. Kopečková and J. Kopeček, *Macromolecules*, 2011, 44, 2481-2488.
43 43. D. Konkolewicz, A. Gray-Weale and S. b. Perrier, *J. Am. Chem. Soc.*, 2009, 131, 18075-18077.
44 44. S. I. Presolski, V. P. Hong and M. G. Finn, *Current Protocols in Chemical Biology*, 2011, 3, 153-162.